

Stoner Magnetism in an Inversion Layer

D. I. Golosov

Department of Physics and the Resnick Institute, Bar-Ilan University, Ramat-Gan 52900, Israel.

Abstract

Motivated by recent experimental work on magnetic properties of Si-MOSFETs, we report a calculation of magnetisation and susceptibility of electrons in an inversion layer, taking into account the co-ordinate dependence of electron wave function in the direction perpendicular to the plane. It is assumed that the inversion-layer carriers interact via a contact repulsive potential, which is treated at a mean-field level, resulting in a self-consistent change of profile of the wave functions. We find that the results differ significantly from those obtained in the pure 2DEG case (where no provision is made for a quantum motion in the transverse direction). Specifically, the critical value of interaction needed to attain the ferromagnetic (Stoner) instability is decreased and the Stoner criterion is therefore relaxed. This leads to an increased susceptibility and ultimately to a ferromagnetic transition deep in the high-density metallic regime. In the opposite limit of low carrier densities, a phenomenological treatment of the in-plane correlation effects suggests a ferromagnetic instability above the metal-insulator transition. Results are discussed in the context of the available experimental data.

Keywords:

inversion layer, Stoner theory, silicon MOSFET, magnetic susceptibility, parallel field

PACS: 73.40.Qv, 75.75.-c, 75.10.Lp

1. Introduction

Recently, there has been much interest in the unusual magnetic and magnetotransport properties of 2-dimensional (2D) electron gas (2DEG) at low densities, as exemplified by the inversion layers in Silicon metal-oxide-semiconductor field effect transistors (Si-MOSFETs) [1, 2], or by GaAs quantum wells. Specifically, indirect magnetisation and susceptibility measurements [3, 4] indicate an increase of low-field magnetic susceptibility with lowering the 2-dimensional carrier density n toward the critical value n_c , corresponding to the metal-insulator transition (MIT). This might imply the presence of a ferromagnetic transition at or near MIT [4], although the situation remains uncertain due to experimental difficulties.

On the theory side, the possibility of ferromagnetism in a 2DEG at low density was raised in the numerical

investigations[5, 6]. Later, a divergence in susceptibility with decreasing n toward n_c was reported based on an advanced renormalisation-group treatment in Ref. [7]. On the other hand, numerical studies based on the diffusion Monte Carlo technique[8] did not find any critical behaviour of susceptibility in a low density two-valley 2DEG.

The effects of finite thickness of the inversion layer on the quasi-2DEG susceptibility were addressed, *e.g.*, in Refs. [9, 10, 11]. In these investigations, the appropriate diagrammatic summations [9] or the Monte-Carlo numerical results [10] are generalised for the quasi-2D case by including the appropriate formfactors[1], whereas for interpreting the experimental findings in Ref. [11], orbital effects of the in-plane magnetic field (which can be non-negligible for a sufficiently thick layer) were invoked.

We note that within the general framework of delocalised-electron magnetism, an important benchmark is provided by Stoner-type mean-field theories.

Email address: Denis.Golosov@biu.ac.il (D. I. Golosov)

The underlying assumption is the presence of a local repulsive interaction between opposite-spin electrons. In the case of a quasi-2DEG, where an important role is played by long-range Coulomb correlations, such an assumption does not at the first sight appear too realistic. Yet we suggest that it might be worthwhile to study it in some detail, especially as a relative simplicity of the situation allows for a full mean-field treatment including the electrostatic effects. We thus aim at generalising the classical Ref. [13] to treat the magnetic response of a silicon inversion layer, where in addition to the long-range Coulomb interaction (which at the mean-field level is included in the effective electrostatic potential), contact (on-site) repulsion between the carriers is also taken into account. We note that in the case of silicon, recent density functional theory results[12] suggest a rather large value of on-site repulsion $U_{on-site} \approx 3eV$. This is somewhat unexpected for a semiconductor with covalent bonds, and perhaps provides an additional motivation for the present study. The validity of our mean-field approach will be discussed elsewhere.

2. Mean-Field Description of an Inversion Layer

Following Ref. [13], we consider an n -doped Si inversion layer, with the value of chemical potential fixed at the top of the valence band E_v of the bulk silicon. We set E_v to be our zero of energy, and we further assume the presence of an acceptor level at $E = E_v = 0$, with the volume density of acceptors N_A . The bottom of conduction band bends from its bulk value $E_c \approx 1.12eV$ (attained far away from the surface, where the transverse co-ordinate z is large and positive) to a variable value $E_{cs} < 0$ at the surface ($z = 0$), which is controlled by the electrostatic potential ϕ_{gate} at the metallic gate,

$$\phi(z=0) \equiv -\frac{1}{e}(E_{cs} - E_c) = -\frac{1}{C}Q_{gate} + \phi_{gate}. \quad (1)$$

Here, we assume that the potential $\phi(z)$ vanishes deep within the bulk (more precisely, at $z > z_d$, where z_d is the depletion layer width); $-e$ is the electron charge, C is the capacitance per unit area of the oxide layer, and Q_{gate} is the (positive) surface charge density at the gate, which exactly compensates the induced charges in the semiconductor: $Q_{gate} = e(n_{\uparrow} + n_{\downarrow} + N_A z_d)$, with n_{\uparrow} (n_{\downarrow}) being the density of the 2DEG carriers with spin up (down). The constant difference in work functions is absorbed into ϕ_{gate} . The value of ϕ at $z > 0$ is found from the (self-consistent) Poisson's equation as

$$\phi(z) = \frac{1}{e}(E_c - E_{cs}) -$$

$$-\frac{4\pi e}{\epsilon}(N_A z_d + n_{\uparrow} + n_{\downarrow})z + \frac{2\pi e}{\epsilon}z^2 N_A + \frac{4\pi e}{\epsilon} \int_0^z dz' \int_0^{z'} [n_{\uparrow}\psi_{\uparrow}^2(z'') + n_{\downarrow}\psi_{\downarrow}^2(z'')] dz'', \quad (2)$$

where $\epsilon \approx 11.9$ is the static dielectric constant of bulk Si. The wave-functions ψ_{α} (with $\alpha = \uparrow, \downarrow$) of the transverse motion are the ground-state eigenfunctions of the effective mean field one-dimensional Hamiltonian (we recall that in the underlying quantum mechanical problem transverse carrier motion separates from the in-plane one, the latter being free):

$$\mathcal{H}_{\alpha} = E_c - \frac{\hbar^2}{2m_{\parallel}} \frac{\partial^2}{\partial z^2} - e\phi(z) + U n_{-\alpha} \psi_{-\alpha}^2(z) - \frac{1}{2} H \sigma_{\alpha\alpha}^z, \quad (3)$$

$$\mathcal{H}_{\alpha} \psi_{\alpha} = E_{0\alpha} \psi_{\alpha}. \quad (4)$$

Here, m_{\parallel} is the transverse effective mass [for Si-(100) surface, $m_{\parallel} \approx 0.916$ in the units of free electron mass m_e], H is the in-plane magnetic field in units of $g\mu_B$ (bare g -factor times Bohr magnetone), and σ^z is the Pauli matrix. Orbital effects of the in-plane field, which have been discussed elsewhere[11, 14], are not included in our \mathcal{H} . U is the contact repulsion (or an s -wave scattering) potential, which is related to the on-site repulsion $U_{on-site}$ on the underlying discrete lattice roughly as $U = a^3 U_{on-site}$ with $a \approx 5.43 \text{ \AA}$ the lattice period. While for the Si-(100) surface two equivalent electron valleys should be taken into account, here we assume that the Hamiltonian is diagonal in the valley index. In writing Eqs. (3–4), we assumed that only the ground states $E_{0\alpha}$ (for $\alpha = \uparrow, \downarrow$) can be populated by the carriers (electric quantum limit [13]).¹ Then the respective carrier densities at zero temperature are given by

$$n_{\alpha} = -2\nu E_{0\alpha} \theta(-E_{0\alpha}), \quad \nu = \frac{m_{\perp}}{2\pi\hbar^2}, \quad (5)$$

where the factor 2 accounts for the valley degeneracy, θ is the Heavyside function, and $m_{\perp} \approx 0.190m_e$ is the effective mass of the in-plane motion. The net carrier density and magnetisation (in units of μ_B) are then

$$n = n_{\uparrow} + n_{\downarrow}, \quad M = \frac{n_{\uparrow} - n_{\downarrow}}{2}. \quad (6)$$

The self-consistent mean field scheme is completed by an equation for the depletion layer width z_d , viz..

$$\frac{2\pi e^2}{\epsilon} N_A z_d^2 = E_c - E_{cs} - \frac{4\pi e^2}{\epsilon} (n_{\uparrow} z_{\uparrow} + n_{\downarrow} z_{\downarrow}), \quad (7)$$

where $z_{\alpha} = \int_0^{\infty} z \psi_{\alpha}^2(z) dz$ is the average value of z for spin-up or spin-down carriers.

¹Generalisation for the high-density region where several transverse-motion levels E_n are active is straightforward.

In the $U = 0, H = 0$ case using an *ansatz*[13, 15]

$$\psi(z) = \sqrt{\frac{b^3}{2}} z \exp(-bz/2) \quad (8)$$

with an appropriate b yields the values of E_0 which agree quite well with numerical solution of Eqs. (3–4). We find a similar behaviour in the $U > 0, H = 0$ unpolarised case, where the equation for b now reads

$$\frac{\hbar^2 b^3}{4m_{\parallel}} + \frac{3}{64} U n b^2 - \frac{12\pi e^2}{\epsilon} \left(N_A z_d + \frac{11}{32} n \right) = 0. \quad (9)$$

The addition of the second term on the l. h. s. results in a slight decrease of the value of b (and hence in an increase of $z_{\uparrow} = z_{\downarrow} = 3/b$) in comparison to the non-interacting case, as can be expected on general grounds.

3. Magnetic susceptibility

Conventional Stoner picture in the uniform three-dimensional case involves the energy shifts of the two spin subbands under the combined effect of H and the Hartree field *without* changing the wave functions. When using the *ansatz* (8) in the case of an inversion layer in the electric quantum limit, this approach yields the following expression for the magnetic susceptibility:

$$\chi_{St} \equiv \frac{\partial M}{\partial H} \Big|_{H \rightarrow 0} = \frac{\nu}{1 - \frac{3}{8} U b \nu}. \quad (10)$$

We note that χ depends on the carrier density n , due to the presence of an n -dependent quantity b in the denominator. This is in turn due to the fact that U is a three-dimensional contact interaction, whereas the two-dimensional contact repulsion between the 2DEG carriers is in general obtained by integrating over z as

$$U_{2D} = U \int_0^{\infty} \psi_{\uparrow}^2(z) \psi_{\downarrow}^2(z) dz. \quad (11)$$

In the unpolarised case, while also using the *ansatz* (8), one obtains $U_{2D} = 3Ub/16$. Since b increases with n [13], so does the susceptibility, Eq. (10) (see below, Fig. 2).

It is however obvious that for $U > 0$ the transverse-motion wave functions $\psi_{\alpha}(z)$ do change when spin polarisation is induced. In order to clarify this, we will first assume that for each spin projection, only the ground state $E_{0\alpha}$ of z -axis motion is populated with carriers. While this assumption is quantitatively adequate only for smaller densities below $3 \cdot 10^{12} \text{ cm}^{-2}$, it allows an easy insight into the generic qualitative behaviour which persists also in a complete (and more cumbersome)

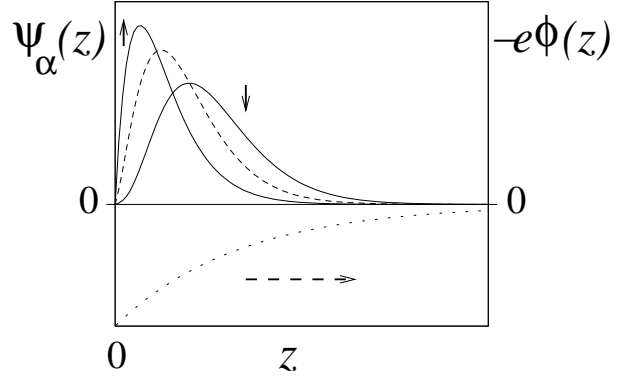


Figure 1: Schematic representation of the effect of spin polarisation on the transverse-motion wave-functions at $U > 0$. While in the unpolarised case spin-up and -down wavefunctions coincide (dashed line), this is no longer true at $M > 0$ (solid lines). Dotted line represents the electrostatic potential energy, $-e\phi(z)$.

multi-level picture needed at higher densities, which we will discuss later.

In the presence of spin polarisation, the Hartree field of spin-up (majority) electrons creates a potential bump for the spin-down electrons [see Eq. (3)], with the result that spin-down electrons are pushed towards larger z . This new spin-down electron distribution in turn creates a (smaller) bump for the spin-up electrons at these larger values of z , as a result pushing the spin-up electrons closer to the surface. This situation is shown schematically in Fig. 1. While for simplicity we show the electrostatic potential $\phi(z)$ as a single dotted line (as if it does not change when polarisation arises), in reality it is affected by the change in wave functions [see Eq. (2)], and the resultant new $\phi(z)$ must be fed back self-consistently into Eq. (3). The interaction energy decreases with decreasing wavefunction overlap, so that sufficiently large U would imply, at the mean field level, a tendency towards ferromagnetism which (unlike in the usual Stoner picture) involves a degree of spatial separation of opposite-spin carriers along the transverse direction.

In order to probe this picture variationally, we write instead of Eq. (8):

$$\psi_{\alpha}(z) = \sqrt{\frac{b_{\alpha}^3}{2}} a_{\alpha} z \sqrt{1 + \gamma_{\alpha} b_{\alpha}^2 z^2} \exp(-b_{\alpha} z/2). \quad (12)$$

Here the parameters γ_{α} and b_{α} control the behaviour of wave function at small and large values of z respectively, whereas a_{α} is a normalisation coefficient. In the absence of polarisation, the coefficients here do not depend on the spin index α . The values of b and γ can be found by minimising the appropriate thermodynamic potential G .

It is somewhat simpler to work this out at a fixed total charge $n + N_A z_d$ and hence fixed E_{cs} [cf. Eq. (1)], as opposed to fixed ϕ_{gate} (while the actual situation corresponds to fixing ϕ_{gate} , the two approaches are equivalent for $M = 0$ or for an infinitesimal M needed when calculating susceptibility). In the unpolarised case, we have

$$G = -n \int_0^\infty \psi(z) \frac{\hbar^2}{2m_\parallel} \frac{\partial^2}{\partial z^2} \psi(z) dz + \frac{n^2}{8v} + nE_c + \frac{Un^2}{4} \int_0^\infty \psi^4(z) dz - \frac{en}{2} \int_0^\infty \psi^2(z) \phi(z) dz - \frac{eN_A}{2} \int_0^{z_d} \phi(z) dz - \frac{1}{2}(n + N_A z_d)(E_c - E_{cs}) \quad (13)$$

Here, the first four terms are transverse and in-plane kinetic energy of the carriers, the band-gap contribution and the interaction energy; the next two terms are the electrostatic energies of carriers and acceptors [see Eq. (2)], and the last term corresponds to the appropriate choice of thermodynamic potential for the case of fixed E_{cs} as explained above. The values of z_d and n are found self-consistently from Eqs. (7) and (5–6), respectively, where in Eq. (5) one has to substitute for $E_{0\alpha}$ the variational energy value,

$$E_0 = - \int_0^\infty \psi(z) \frac{\hbar^2}{2m_\parallel} \frac{\partial^2}{\partial z^2} \psi(z) dz + E_c + \frac{Un}{2} \int_0^\infty \psi^4(z) dz - \frac{e}{2} \int_0^\infty \psi^2(z) \phi(z) dz. \quad (14)$$

Further details can be found in the Appendix.

We note that even in an unpolarised case at $U = 0$, the wavefunction (12) represents an improvement in comparison to Eq. (8), as indicated by a non-zero value of the coefficient $\gamma > 0$ found from the energy minimisation. With increasing U , the value of γ decreases but stays positive throughout physically relevant range of parameter values. When a polarisation is induced, $M \neq 0$, the parameters of the wave function (12) depend on the spin index. As long as polarisation is small, $M/n \ll 1$, we write to leading order

$$b_\alpha = (1 \pm \beta)b, \quad \gamma_\alpha = \gamma \pm \delta. \quad (15)$$

Collecting the leading-order corrections to the self-consistent electrostatic energies of carriers and acceptors, as well as to the variational energies $E_{0\alpha}$ of the transverse motion, enables one to evaluate the susceptibility. The resultant expression is somewhat cumbersome and is given in the Appendix [see Eq. (A.6)].

Results are presented in Fig. 2 (a), where the dashed line corresponds to the variational calculation based on Eq. (12). The computed value of χ exceeds that of

the non-interacting case (Pauli susceptibility, $\chi \equiv \nu$ in our notation), and increases with increasing n . One can see that the variational calculation somewhat overestimates the tendency toward ferromagnetism, suggesting a transition at $n_v \approx 1.9 \cdot 10^{13} \text{ cm}^{-2}$, whereas the numerical solution of mean-field equations [including the Schrödinger equation (4); see solid line in Fig. 2 (a)] yields the critical value $n_1 \approx 5.4 \cdot 10^{13} \text{ cm}^{-2}$. Importantly, the “variational Stoner” approach, using Eqs. (8) and (10) (dotted line in Fig. 2 (a)), strongly underestimates χ and misses the transition. Indeed, the ratio χ_{St}/ν slowly increases with density, reaching the value of 2 only at $n \sim 5 \cdot 10^{14} \text{ cm}^{-2}$ (this is for $U = 10^{-33} \text{ erg/cm}^3$, as used in Fig. 2); on the other hand, we find that for χ_{St} to diverge at $n = n_1$, one must increase the value of U to $U \approx 4.0 \cdot 10^{-33} \text{ erg/cm}^3$, *i.e.*, by a factor of 4.

If one neglects the effect of wavefunction change, depicted schematically in Fig. 1, the Stoner criterion of ferromagnetism is determined precisely by the divergence of χ_{St} , Eq. (10) as

$$2\nu U_{2D} > 1 \quad (16)$$

i.e., takes on a purely-2D form. We see that treating the z -axis motion properly (which includes taking into account interaction-induced wave functions change in the presence of spin polarisation) *relaxes* the Stoner criterion.

The inset in Fig. 2 (a) shows the numerical results for the behaviour of spin polarisation degree $2M/n$ above the transition. It is seen that M increases continuously, and the transition appears to be second-order. This is an important difference from a conventional Stoner theory in two dimensions where (in the case of a perfectly flat density of state and at a fixed n , and at the level of the present treatment) the total energy at the critical point does not change as $2M/n$ is varied from 0 to 1, and a fully spin-polarised state is stabilised beyond the transition, resulting in a magnetisation jump. In reality, however, the opposite-spin transverse wave functions overlap decreases with increasing M (cf. Fig. 1), hence the effective two-dimensional repulsion, Eq. (11) and the Hartree field also decrease, resulting in a smooth transition.

As explained above, the results plotted in Fig. 2 (a) are only indicative, as in reality at those densities where the critical behaviour is suggested more than one quantum-mechanical level of the z axis motion is populated. In Fig. 2 (b), we show the results of full numerical calculation of susceptibility. These are obtained by solving Eqs. (2–5), generalised for the case of multiple active levels. With increasing density, carriers begin to

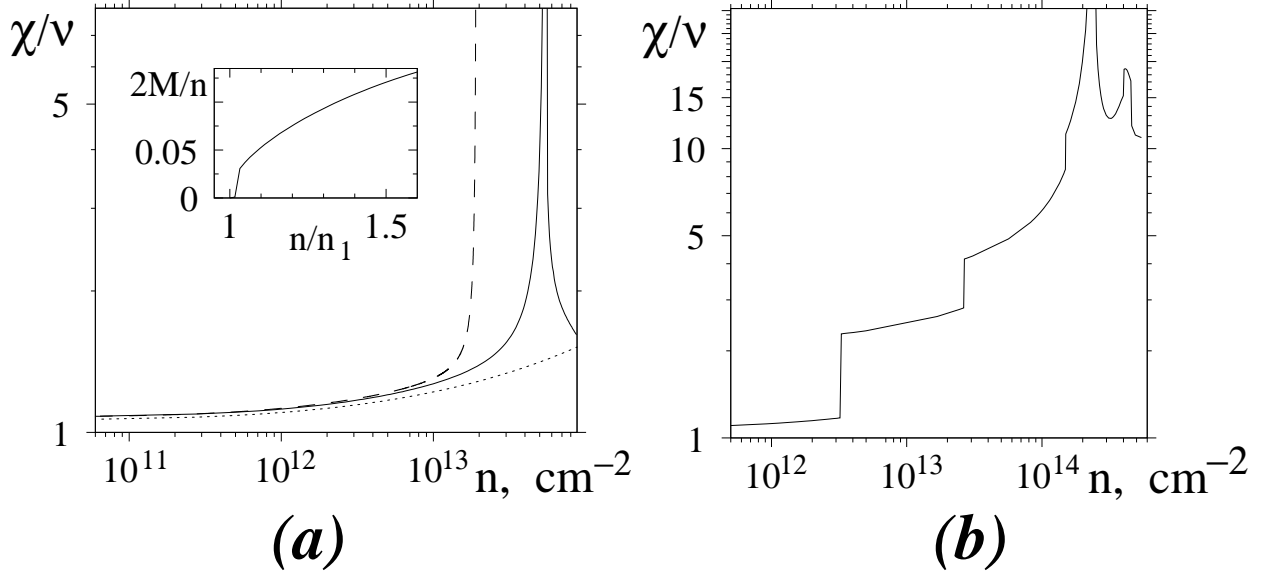


Figure 2: Magnetic susceptibility χ as a function of inversion-layer carrier density n . (a) Results assuming single populated level for the z -axis motion. Solid, dashed, and dotted line correspond respectively to the numerical solution of the mean-field equations, variational calculation based on Eq. (12), and the “Stoner” value calculated using Eqs.(8) and (10). The inset shows the numerical solution result for the degree of spin polarisation $2M/n$, which differs from zero above the corresponding critical value, $n_1 \approx 5.4 \cdot 10^{13} \text{ cm}^{-2}$. The parameter values are $N_A = 10^{15} \text{ cm}^{-3}$ and $U = 10^{-33} \text{ erg/cm}^3$, the latter corresponding roughly to $U_{\text{on-site}} = 4\text{eV}$. (b) Numerical results of the full multi-level calculation, showing transition at $n_0 \approx 2.4 \cdot 10^{14} \text{ cm}^{-2}$.

populate the 2nd, 3rd, 4th, and 5th level at $n \approx 3.2 \cdot 10^{12} \text{ cm}^{-2}$, $n \approx 2.6 \cdot 10^{13} \text{ cm}^{-2}$, $n \approx 1.5 \cdot 10^{14} \text{ cm}^{-2}$, and $n \approx 4.0 \cdot 10^{14} \text{ cm}^{-2}$, respectively. This gives rise to the vertical steps in susceptibility, which are clearly visible in Fig. 2 (b). Aside from these, the overall behaviour is qualitatively similar to the single-level results of Fig. 2 (a), although the actual *mean-field critical density for the ferromagnetic transition*, $n_0 \approx 2.4 \cdot 10^{14} \text{ cm}^{-2}$, is larger than n_1 . At $n = n_0$, we find 4 active levels for each spin projection. The increase of critical density as compared to the single-level results of Fig. 2 (a) is due to a broader spatial spread of higher-level wavefunctions (which reduces both the effective 2D interaction and the wavefunction change under the effect of magnetic field). Note that in Fig. 2, variational results are presented for the single-level case only, as the required calculations become more cumbersome in the case of multiple occupied levels.

3.1. Phenomenological treatment of correlations near MIT

So far, we found that the magnetic susceptibility χ increases with increasing density n , with a transition to ferromagnetism deep inside the high-density metallic region. An important underlying assumption was that the in-plane carrier motion is free, which is no longer

adequate for smaller densities close to MIT. Indeed, in this region the dominant role is played by the in-plane Coulomb correlations, as indicated by the measure of the interaction strength, $r_s = m_{\perp} e^2 / (\epsilon \hbar^2 \sqrt{\pi n})$, exceeding unity. Very recently, it has been suggested[16] that the available data at low densities can be described by a phenomenological model of a 2D Fermi gas with a renormalised in-plane mass:

$$\tilde{m}_{\perp} = m_{\perp} \frac{n}{n - n_c}. \quad (17)$$

The Pauli-like in-plane magnetic susceptibility would then be[16]

$$\chi_P = \tilde{\nu}, \quad \tilde{\nu} = \frac{\tilde{m}_{\perp}}{2\pi\hbar^2}. \quad (18)$$

When n approaches n_c from above, χ_P increases because of the effective band narrowing, which does not necessarily imply a magnetic instability (in agreement also with Ref. [7]).

Since there appears to be no reason to expect that the *transverse* motion of carriers is affected by the correlations, we suggest that the effects of a short-range U can be taken into account by substituting $\tilde{\nu} \rightarrow \nu$ in our treatment as described above. It is readily seen that, for example, the variational Stoner susceptibility (10) would

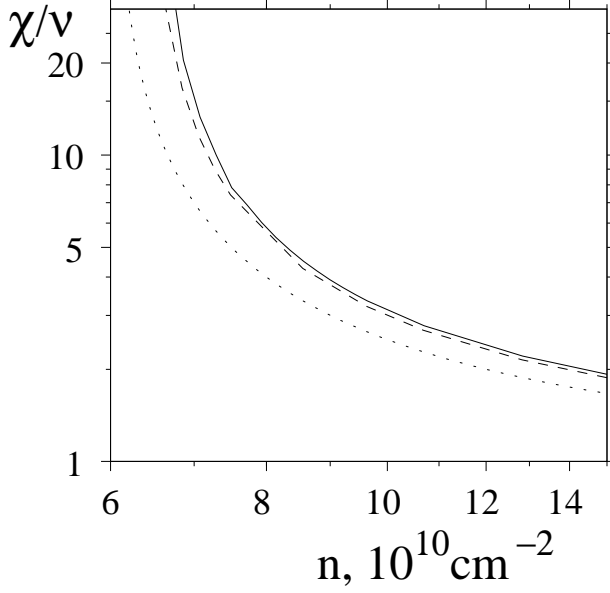


Figure 3: Magnetic susceptibility χ divided by the bare density of states ν [see Eq. (5)] at low densities. In-plane carrier mass is renormalised according to Eq.(17). Solid, dashed, and dotted line correspond respectively to the numerical solution of the mean-field equations, “Stoner” susceptibility calculated using Eqs.(8),(10) with $\nu \rightarrow \tilde{\nu}$, and Pauli susceptibility (18). The parameter values are $N_A = 10^{15} \text{ cm}^{-3}$, $U = 10^{-33} \text{ erg/cm}^3$, and $n_c = 6 \cdot 10^{10} \text{ cm}^{-2}$.

diverge at $n = n_S$, corresponding to a zero of the denominator. For the purpose of an estimate we may use a non-interacting ($U = 0$) value of $b(n)$ [13], yielding an equation

$$\frac{3}{4} U \nu \frac{n_S}{n_S - n_c} \left[\frac{6m_{||}\pi e^2}{\epsilon \hbar^2} \left(N_A z_d + \frac{11}{32} n_S \right) \right]^{1/3} = 1. \quad (19)$$

This suggests that a ferromagnetic state is stabilised at $n_c < n < n_S$. Further refinement can be obtained by using a more adequate variational *ansatz* such as (12), or by solving the mean-field equations numerically. This is illustrated in Fig. 3.

Indeed, we see that while χ_P , Eq. (18), does not show any divergence above n_c , both the variational Stoner result and the numerical solution suggest a transition (at $n_* \approx 1.08 n_c$ for numerical and at $n_S \approx 1.07 n_c$ for variational Stoner; this is for the value of U used in Fig. 3). While the two follow each other rather closely in this regime, the numerical result for χ (and hence for the density value at transition) is larger than the variational one, mostly due to a pronounced difference between the exact transverse wavefunction and the variational one [given by Eq. (8)] in this regime. As explained above, the transition is expected to be second-order. Indeed, numerical results imply that $M(n)$ is continuous

at the transition point, $n = n_*$, and rapidly increases with decreasing density, reaching full spin polarisation at $n_F > n_c$. Full spin polarisation is then sustained in the region $n_c < n < n_F$.

Alternatively, taking into account the accuracy of experimental data, it appears possible that the actual MIT takes place at the point n_F , whereas n_c , which enters Eq. (17), plays the role of an asymptotically defined parameter (a point where the effective mass would have diverged).

4. Discussion

We constructed a Stoner-type theory of magnetism for electrons in an inversion layer, addressing both the behaviour of the system in the metallic high-density region and the correlated low-density regime immediately above the metal-insulator transition. While we specifically aimed at describing Si-(100) MOSFETs, our results are expected to be qualitatively relevant for other 2D electron systems of finite thickness. These general conclusions are: (i) At higher densities, proper treatment requires taking into account the wave function change under the applied in-plane magnetic field (see Fig. 1). This effect leads to an increased susceptibility in the paramagnetic state, and enhances the tendency toward ferromagnetism. As a result, the Stoner criterion is somewhat relaxed in comparison to a more conventional treatment, which in turn may give rise to a ferromagnetic transition. (ii) Even though the overall behaviour at low densities is dominated by long-range Coulomb forces, the magnetic susceptibility can be significantly affected by the on-site carrier repulsion, which is of course always present.

We close with a brief summary of our results for a silicon MOSFET. In the high-density metallic regime, when one neglects the in-plane Coulomb correlations (main body of Sec. 3), the relaxation of the Stoner criterion translates into a lower value of critical density corresponding to a ferromagnetic transition (in comparison to the conventional Stoner approach). Still, the transition to ferromagnetism occurs at rather large n , and it is far from clear whether the corresponding values can be reached in case of Si-MOSFETs. However, the increase of susceptibility with increasing n should perhaps be observable at large yet readily accessible densities, $n \gtrsim 10^{12} \text{ cm}^{-2}$.

Describing the magnetic response of the system at lower densities close to the metal-insulator transition requires taking into account the strongly-correlated nature of the 2DEG in this limit. This was carried out at a phenomenological level in sec. 3.1, and results suggest a

ferromagnetic instability above the metal-insulator transition. This finding contributes to the on-going debate in the literature[3, 4].

The mean-field transition to ferromagnetism is found to be continuous in all cases, and a sublinear behaviour of $M(H)$ at larger H is anticipated (due to decreasing wavefunction overlap). Another important and novel feature of our approach is the spatial separation (in the transverse direction) which arises between opposite-spin carriers in the ferromagnetic case or whenever spin polarisation is induced (the average values of the transverse coordinate of spin-up and -down electrons then differ, $z_\uparrow < z_\downarrow$). This issue will be addressed in more detail elsewhere.

5. Acknowledgements

The author takes pleasure in thanking R. Berkovits, K. A. Kikoin, B. D. Laikhtman, S. V. Kravchenko, I. Shlimak, and L. D. Shvartsman for enlightening discussions. This work was supported by the Israeli Absorption Ministry.

Appendix A. Details of the variational calculation based on Eq. (12)

As a first step, one has to determine the values of the wavefunction parameters b and γ in the unpolarised case by minimising the thermodynamic potential G , Eq. (13). Evaluating all terms in Eqs. (13) and (14) in the usual limit of $z_\alpha \ll z_d$ and differentiating, we find

$$b^2 \frac{\hbar^2 a^2}{2m_\parallel} \left[\Gamma - \frac{1}{2} + 2\gamma \right] + \frac{3}{2^{12}} bnU(69\xi^2 - 210\xi + 205) - \frac{12\pi e^2 N_A z_d \xi}{\epsilon b} - \frac{3\pi e^2 n}{512b\epsilon} (435\xi^2 - 286\xi + 555) = 0, \quad (\text{A.1})$$

$$b^2 \frac{\hbar^2 a^2}{4m_\parallel} \left[-2 - 6a^2 + 24\gamma a^2 + \frac{\Gamma}{2\gamma} (1 + 24\gamma a^2) + \frac{\Omega}{2\gamma^2} \right] = \frac{3}{256} bnUa^4(69\xi - 105) + \frac{96\pi e^2 N_A z_d}{b\epsilon} a^4 + \frac{3}{32} \frac{\pi e^2 n}{b\epsilon} a^4 (435\xi - 143). \quad (\text{A.2})$$

Here, the quantities Γ and Ω depend only on γ , and are expressed in terms of sine and cosine integrals:

$$\Gamma = \frac{1}{\sqrt{\gamma}} \left(\text{ci} \frac{1}{\sqrt{\gamma}} \sin \frac{1}{\sqrt{\gamma}} - \text{si} \frac{1}{\sqrt{\gamma}} \cos \frac{1}{\sqrt{\gamma}} \right), \quad (\text{A.3})$$

$$\Omega = \text{ci} \frac{1}{\sqrt{\gamma}} \cos \frac{1}{\sqrt{\gamma}} + \text{si} \frac{1}{\sqrt{\gamma}} \sin \frac{1}{\sqrt{\gamma}}; \quad (\text{A.4})$$

$a = (1 + 12\gamma)^{-1/2}$ is the normalisation coefficient in Eq. (12) at $m = 0$, and ξ is defined according to $\xi = a^2(1 + 20\gamma)$, so that $z_\uparrow = z_\downarrow = 3\xi/b$. Eqs. (A.1–A.2) must be solved numerically, together with Eqs. (7) and (5–6).

When an infinitesimal in-plane magnetic field H is applied, the spin-up and -down wavefunctions begin to differ from each other according to Eq. (15). This effect, along with the Zeeman splitting of the spin subbands, contributes to the magnetisation,

$$M = \left[(69\xi^2 - 210\xi + 205) \frac{3bnU\gamma}{2048} \beta + (69\xi - 105)a^4 \times \frac{3bnU\gamma}{128} \delta + \nu H \right] \left[1 - \frac{3bU\gamma}{512} (69\xi^2 - 210\xi + 205) \right]^{-1}. \quad (\text{A.5})$$

The thermodynamic potential acquires a correction, $G \rightarrow G + \Delta G$, which is quadratic in β , δ , and H . The values of β and δ can be found by minimising ΔG , yielding magnetisation M [with the help of Eq. (A.5)], and hence the susceptibility χ . A straightforward, if somewhat tedious, calculation yields

$$\chi = \left[1 - \frac{3bU\gamma}{512} (69\xi^2 - 210\xi + 205) - K \right]^{-1} \quad (\text{A.6})$$

Here the first two terms correspond to the Stoner susceptibility, computed using the wavefunctions (12) of the unpolarised case [instead of (8); cf. Eq. (10)], whereas the quantity

$$K = \frac{9\gamma b^2 n U^2}{2^{16}(AB - C^2)} \left[\frac{A}{64} (69\xi^2 - 210\xi + 205)^2 + 4a^8 B \times \right. \\ \left. \times (69\xi - 105)^2 - \frac{a^4 C}{2} (69\xi^2 - 210\xi + 205)(69\xi - 105) \right]$$

accounts for the field-induced change of the spin-up and down wavefunctions, as illustrated by Fig. 1. The coefficients A , B , and C are given by

$$A = \frac{\hbar^2 a^2 n b^2}{2m_\parallel} \left[\Gamma \left(\frac{6a^2}{\gamma} + \frac{3}{8\gamma^2} - \frac{1}{8\gamma^3} + 144a^4 \right) + \Omega \times \right. \\ \left. \times \left(\frac{6a^2}{\gamma^2} + \frac{5}{8\gamma^3} \right) - 24a^2 + \frac{1}{8\gamma^3} - 72a^4 + 288a^4 \gamma \right] - \\ - \frac{3\pi e^2 n^2}{4\epsilon b} (1305\xi - 429)a^6 - \frac{2^8 \cdot 9\pi e^2 N_A z_d n a^6}{\epsilon b} + \\ + \frac{9}{64} U b n^2 (95 - 69\xi)a^6, \\ B = \frac{\hbar^2 a^2 n b^2}{2m_\parallel} \left(\Gamma - \frac{1}{2} + 2\gamma \right) - \frac{3\pi e^2 n^2}{2^9 \epsilon b} (975\xi^2 - 2638\xi + \\ + 1215) + \frac{24\pi e^2 N_A z_d n \xi}{\epsilon b} + \frac{9}{2^{11}} U b n^2 (-199\xi^2 + 510\xi - \\ - 375),$$

$$C = \frac{\hbar^2 a^2 n b^2}{2m_{\parallel}} \left[-\Gamma \left(\frac{1}{2\gamma} + 12a^2 \right) + 2 + 6a^2 - 24a^2 \gamma^2 - \frac{\Omega}{2\gamma^2} \right] - \frac{3\pi e^2 n^2}{64\epsilon b} (435\xi - 751)a^4 - \frac{96\pi e^2 N_A z_d n a^4}{\epsilon b} + \frac{45}{32} U b n^2 a^4.$$

References

- [1] T. Ando, A. B. Fowler, and F. Stern, *Rev. Mod. Phys.* **54**, 437 (1982).
- [2] S. V. Kravchenko and M. P. Sarachik, *Rep. Prog. Phys.* **67**, 1 (2004), and references therein.
- [3] O. Prus, Y. Yaish, M. Reznikov, U. Sivan, and V. Pudalov, *Phys. Rev.* **B67**, 205407 (2003).
- [4] S. V. Kravchenko, A. A. Shashkin, S. Anissimova, A. Venkatesan, M. R. Sakr, V. T. Dolgoplov, and T. M. Klapwijk, *Ann. Phys.* **321**, 1588 (2006); A. A. Shashkin, S. Anissimova, M. R. Sakr, S. V. Kravchenko, V. T. Dolgoplov, and T. M. Klapwijk, *Phys. Rev. Lett.* **96**, 036403 (2006).
- [5] B. Tanatar and D. M. Ceperley, *Phys. Rev.* **B39**, 5005 (1989).
- [6] C. Attaccalite, S. Moroni, P. Gori-Giorgi, and G. B. Bachelet, *Phys. Rev. Lett.* **88**, 256601 (2002).
- [7] A. Punnoose and A. M. Finkelstein, *Science* **310**, 289 (2005).
- [8] M. Marchi, S. De Palo, S. Moroni, and G. Senatore, *Phys. Rev.* **B80**, 035103 (2009).
- [9] Y. Zhang and S. Das Sarma, *Phys. Rev.* **B72**, 075308 (2005).
- [10] S. De Palo, M. Botti, S. Noroni, and G. Senatore, *Phys. Rev. Lett.* **94**, 226405 (2005).
- [11] E. Tutuc, S. Melinte, E. P. De Poortere, M. Shayegan, and R. Winkler, *Phys. Rev.* **B67**, 241309 (2003).
- [12] V. L. Campo, Jr., and M. Cococcioni, *J. Phys.: Condens. Matter*, **22**, 055602 (2010).
- [13] F. Stern, *Phys. Rev.* **B5**, 4891 (1972).
- [14] S. Das Sarma and E. H. Hwang, *Phys. Rev. Lett.* **84**, 5596 (2000).
- [15] F. F. Fang and W. E. Howard, *Phys. Rev. Lett.* **16**, 797 (1966).
- [16] V. T. Dolgoplov, *JETP Lett.* **101**, 282 (2015) [*Zh. Eksp. Teor. Fiz. Pis'ma Red.*, **101**, 300 (2015)].